1971

Laser interferometric holography investigation of free convection about a vertical plate of non-uniform temperature

Richard Kenneth Thomson

Department:

LASER INTERFEROMETRIC HOLOGRAPHY INVESTIGATION OF FREE CONVECTION ABOUT A VERTICAL PLATE OF NON-UNIFORM TEMPERATURE

BY

RICHARD KENNETH THOMSON, 1948-

A THESIS

Presented to the Faculty of the Graduate School of the

UNIVERSITY OF MISSOURI-ROLLA

In Partial Fulfillment of the Requirements for the Degree

MASTER OF SCIENCE IN MECHANICAL ENGINEERING

1971

Approved by

R L Reed (Advisor) A. S Crosbie

A K Ryler

ABSTRACT

An experimental investigation was conducted using a holographic interferometer to detect the temperature variation in a free convection boundary layer about a vertical heated plate. The heated plate was non-isothermal and investigations were conducted for four temperature distributions; the maximum plate temperature ranged from 200F to 493F. Photographs were taken of the fringe patterns and boundary layer thickness measurements, as well as temperature measurements, were made. A theoretical model was constructed by applying the integral method to the energy and momentum equations. The experimental values agree quite well with this model. The advantages of the holographic interferometer over other systems are discussed.

TABLE OF CONTENTS

Page

ABSTRACT ii

LIST OF ILLUSTRATIONS iv

LIST OF TABLES v

LIST OF SYMBOLS vi

I. INTRODUCTION 1

II. REVIEW OF LITERATURE 3

A. Principles of Interferometry 3

B. Optical Temperature Methods 4

1. The Modified Schlieren 4

2. The Mach-Zehnder Interferometer 7

C. Holographic Interferometer 9

III. EXPERIMENTAL APPARATUS 11

A. Apparatus 11

1. The Table 11

2. The Heated Plate 11

3. The Optical Components 15

B. Experimental Procedure 17

IV. THEORETICAL MODEL 21

V. RESULTS AND DISCUSSION 29

VI. CONCLUSIONS 52

BIBLIOGRAPHY 54

VITA 56

LIST OF ILLUSTRATIONS

Figure		Page
1	Schlieren System	6
2	The Table	12
3a	The Heated Plate	13
3b	Thermocouple Jacket	13
4	Table Layout Sketch	16
5	Table Layout Photograph	18
6	Boundary Layer for Plate 1	31
7	Boundary Layer for Plate 2	32
8	Boundary Layer for Plate 3	33
9	Boundary Layer for Plate 4	34
10	Comparison Sketches for Plate 1	36
11	Comparison Sketches for Plate 2	37
12	Comparison Sketches for Plate 3	38
13	Comparison Sketches for Plate 4	39
14	Temperature Distribution in the Boundary Layer for Plate 1	43
15	Temperature Distribution in the Boundary Layer for Plate 2	44
16	Temperature Distribution in the Boundary Layer for Plate 3	45
17	Temperature Distribution in the Boundary Layer for Plate 4	46
18	Front Edge Boundary Layer.	48
19	Surface Fringes	50

LIST OF TABLES

Table Page

I. Data 30

LIST OF SYMBOLS

A	a constant (dimensionless) see eqn. (6)
b	plate width (ft)
B	coefficient of thermal expansion ($\frac{1}{F}$)
$C_o, C_1, ..$	thermal B. L. coefficients (ft^{1-m}, ft^{1-p}, etc.)
$D_o, D_1, ..$	velocity B. L. coefficients ($\frac{ft^{1-n}}{sec}$, $\frac{ft^{1-s}}{sec}$, etc.)
g	acceleration due to gravity ($\frac{ft}{sec^2}$)
L	length of the plate (ft)
m,n,p,s	arbitrary exponents (dimensionless) see eqns.(13,14 19)
Pr	Prandtl number (dimensionless)
qw(x)	local heat transfer rate ($\frac{Btu}{hr}$)
Q	overall heat transfer rate ($\frac{Btu}{hr}$)
r	arbitrary exponent (dimensionless) see eqn. (6)
T	boundary layer temperature (F)
$T_w(x)$	wall temperature (F)
T_{wa}	average wall temperature (F)
T_∞	ambient temperature (F)
u	velocity in x direction (ft/sec)
w	ficticious velocity parameter (ft/sec)
w_o, w_1, w_2	perturbation functions for w (ft/sec)
x	coordinate along the plate (ft)
y	coordinate perpendicular to the plate (ft)

LIST OF SYMBOLS (continued)

GREEK SYMBOLS

α	thermal diffusivity (ft^2/hr)
δ	thermal boundary layer thickness (ft)
$\delta_o, \delta_1, \delta_2$	perturbation functions for δ (ft)
$\theta_w(x)$	wall-ambient temperature difference (F)
θ_{wo}	θ_w evaluated at x = 0; a constant (F)
ν	kinematic viscosity (ft^2/sec)

I. INTRODUCTION

Since the advent of the laser in 1962, its span of application has seemed to increase daily. Non-destructive applications of the laser range from differential strain measurement, to three dimensional photography, to the measurement of vibrations to measurement of flow fields. In spite of these creative innovations, the use of holography in the field of heat transfer has, for the most part, been overlooked. There have been a few inconclusive experiments made and photographs published but, as yet, to the author's knowledge, nothing of significance has appeared in the literature.

The field of optical temperature measurement has thus far been dominated by the Mach-Zehnder interferometer. The fringes obtained from the Mach-Zehnder are very distinct, but the instrument does have its limitations. This instrument is extremely expensive, which places severe limitations on its use. The Mach-Zehnder requires precision alignment, an essentially dust-free environment, and optically perfect windows in the test section; all of these are limitations on the use of this instrument.

It is the purpose of this paper to demonstrate the application of holography to temperature measurement and to show how these measurements correlate to the established

theory. It will be shown that the holographic interferometer produces fringes of a quality at least equal to the Mach-Zehnder, has none of the limitations described in the preceding paragraph, and has certain advantageous characteristics available with no other interferometric system.

The author is deeply grateful to Dr. R.L. Reisbig for the conception of this experiment and his invaluable assistance in attaining its completion. The author is also indebted to Dr. A.K. Rigler for his assistance in holographic construction and to Dr. A.L. Crosbie for his contributions in the development of the theoretical model.

This research was supported by a Themis research grant under the direction of Dr. J. Kassner and this financial assistance is greatly appreciated.

II. REVIEW OF LITERATURE

A. Principles of Interferometry

The same basic principles of optics apply to all interferometric systems used to investigate fluid properties, so it is appropriate that the discussion of these principles precede any discussion of the individual systems themselves.

If a monochromatic light beam passes through an undisturbed region, it likewise, will be undisturbed. However, if the air is heated (or cooled) it will cause a density change which is equivalent to a change in refractive index. This refractive index change causes a bending of the light proportional to the magnitude of the change. This disturbed beam interferes with an undisturbed reference beam causing the formation of fringes. The fringes are iso-index of refraction lines.

The Dale-Gladstone[1] law states that the following relationship exists between the index of refraction n and the density ρ:

$$(1 + K_\lambda \rho_m)L = n_m L,$$

where the subscript "m" indicates the properties of any fringe, K_λ is the Dale-Gladstone constant, and L is the

---

*Superscripts indicate references cited in Bibliography

length of the test section. The path length difference between successive maxima fringes is one wave length (λ). Therefore,

$$(1 + K_\lambda \rho_m)L - (1 + K_\lambda \rho_{m+1})L = n_m L - n_{m+1} L = \lambda$$

or

$$\rho_{m+1} = \rho_m - \frac{n_m - n_{m+1}}{K} = \rho_m - \frac{\lambda}{K_\lambda L}$$

and the density change between adjavent fringes is

$$\Delta\rho = (\rho_m - \rho_{m+1}) = \frac{\lambda}{K_\lambda L} ,$$

which is a constant for a given system. [1] For constant pressure, the density change is proportional to a temperature change. Hence, the fringes are constant temperature lines and the measurable temperature variation is influenced not only by the wave length of illumination, but also by the length of the test section that the light must traverse.

B. Optical Temperature Methods

There are a number of interferometers currently in use, however some are more applicable to free convection problems than others. Two interferometric systems will be described here: 1) the Modified Schlieren, and 2) the Mach-Zehnder interferometer.

1) The Modified Schlieren

In order to understand the workings of the modified

Schlieren, one must first understand the workings of the basic Schlieren system. The basic Schlieren system is pictured in Figure 1(a). Light from a pinhole P is allowed to fall on a lens L_1, and is focused to the image point I. If a lens L_2 is placed just past the image point, it can be used to obscure a large portion of the illumination beam, leaving only a small portion for background illumination.

Consider now the insertion of an elemental volume dv with a different index of refraction. If this refractive index change causes an upward deflection of the beam, it will no longer be obscured by the knife edge E and there will be a one to one correspondence between the volume dv and the image seen on the screen. This is the conventional Schlieren system.

The modified Schlieren is shown in Figure 1(b). The principle modification is the use of a collimating lens in place of the converging lens L_1. The variable density region causes the production of a phase distribution just beyond the test section. This phase distribution can be converted to an amplitude variation by forming an image of this distribution with a convex lens. Some form of absorbing material must be inserted in the focal plane to block the central maximum of the Fraunhofer defraction pattern resulting from the free field.

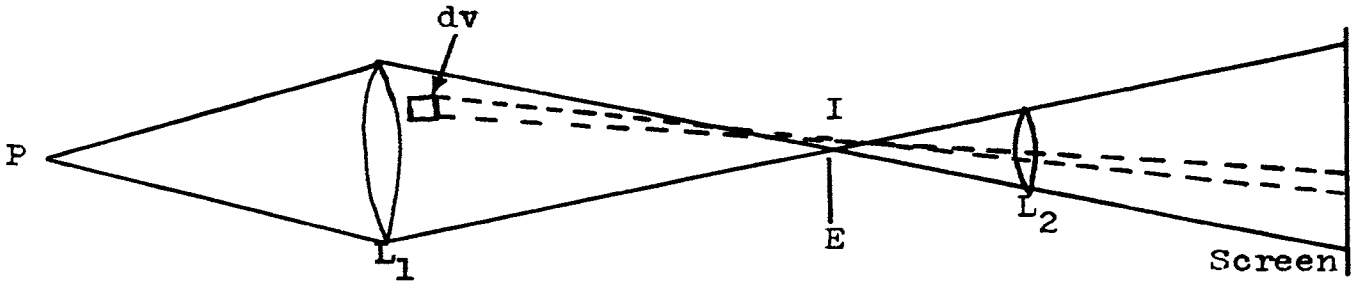

a) Basic Schlieren

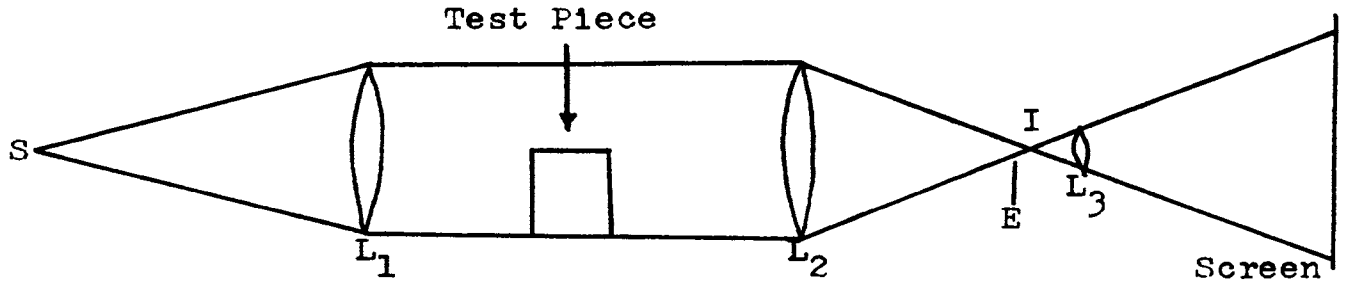

b) Modified Schlieren

Fig. 1 Schlieren System

With this system, the same information can be obtained as is obtained with the Mach-Zehnder, at considerably less expense[1]. This system still has a number of undesirable traits, however. The lenses and mirrors must be of highest optical quality and be kept in essentially a dust-free environment. The test section must also have optically perfect windows reducing the use of the instrument or increasing the expense of the experiment. Another problem in the use of this system is the precision alignment of the knife-edge and absorptive material that is necessary in order to effect the appearance of the fringe system. Many of these same problems are exhibited by the Mach-Zehnder which, as has been previously mentioned, has dominated the field of optical heat transfer measurement.

2) The Mach-Zehnder Interferometer

The operation of the Mach-Zehnder can be rather simply stated. The operating portion of the Mach-Zehnder consists of two silvered and two half-silvered mirrors on four corners of a rectangle. The totally silvered mirrors are located on one diagonal while the half-silvered occupy the other diagonal. This configuration creates two beams, one which passes through the test section while the other passes directly to the viewing screen and serves as a reference beam. The interference between these two beams creates the interference fringes.

This statement of the operation of the Mach-Zehnder is deceptively simple. The expression for the basic positions of the Mach-Zehnder involves five differential equations in twelve unknowns. The interferometer itself is an extremely sophisticated piece of equipment, and the devices necessary for alignment are equally sophisticated. Optical perfection is needed in all components along with the necessity of maintaining a dust-free environment in order to maintain this perfection. The cost of this precision instrument is understandably high, which limits the use of this instrument to the privileged few. For a more detailed explanation of the operation of the Mach-Zehnder interferometer (MZI) the reader is directed to the literature.[2]

A number of in depth studies have been conducted using the MZI. These studies include the investigation of the constant wall temperature convective boundary layer, the heated cylinder, and the study of water flowing between two isothermal walls, one hotter and one cooler than the fluid temperature. These studies are complete with the theoretical boundary layer solutions, and thorough explanations of the photographs. These investigations are too lengthy to reproduce here and the reader is again referred to the literature.[2,3]

In spite of the expense of the MZI and the difficulty of alignment, the Mach-Zehnder has dominated the field of

optical heat transfer because of the previously unparalleled quality of the fringe patterns obtained. The fringes obtained by the holographic interferometer are of equal quality and, in addition, the holographic interferometer is able to record three dimensional information obtainable with no other interferometer.

C. Holographic Interferometer

The statement concerning the lack of holographic applications to heat transfer was not intended to imply that a holographic interferometer had not yet been conceived. In fact, a number of holographic interferometers have been devised, primarily for the viewing of Moire strain fringes. The holographic interferometer is a differential interferometer, that is, it measures extremely small changes in optical path length. One of the most widely used techniques is one which involves double exposure of a photographic plate.

The principle involved is quite simple. In fact, it is the same principle that applies to the study of convection. The primary variation in the holographic interferometer is that two exposures are required. The first exposure is a reference exposure of the undisturbed object. The disturbance, in this case is caused by some type of loading, which causes an optical path length change, which is recorded by the second exposure. The interaction between these two exposures causes the formation of fringes.

This same technique has been applied to heat transfer by Heflinger, Wuerker and Brooks.[4] They describe the basic advantages of the holographic interferometer as they have applied it to both aerodynamics and heat transfer. They have included a number of photographs in the article, foremost of which is the now widely reproduced light bulb picture which exhibits density variations due to heating of the filament. A number of other articles[5,6] have produced similar photographs, but no one has conducted an in depth investigation of temperature measurement. Herein lies that investigation.

III. EXPERIMENTAL APPARATUS AND PROCEDURE

A. Apparatus

The apparatus can best be described in three parts: 1) the table; 2) the heated plate; and 3) the optical components.

1. The Table

A stable, vibration free working surface is essential for the production of holograms. The table as it was designed and constructed by the author, is pictured in Figure 2. It consists of two aluminum slabs 12 feet by 4 feet by 1 1/2 inches mounted on inner-tubes, and separated by legs of Bakelite that were 39 inches by 8 inches by 6 inches. The inner-tubes isolate the table from any floor vibrations that might otherwise destroy the fringes. The aluminum plates and the Bakelite legs were used because the materials were available. Concrete blocks, supporting any flat surface, would work as well. The essential item is stability of the system during exposure of the photographic plate.

2. The Heated Plate

The heated plate, as it was designed and constructed by the author, is pictured in Figure 3(a). The plate consists of a 8 inch by 4 inch by 1/4 inch piece of cartridge

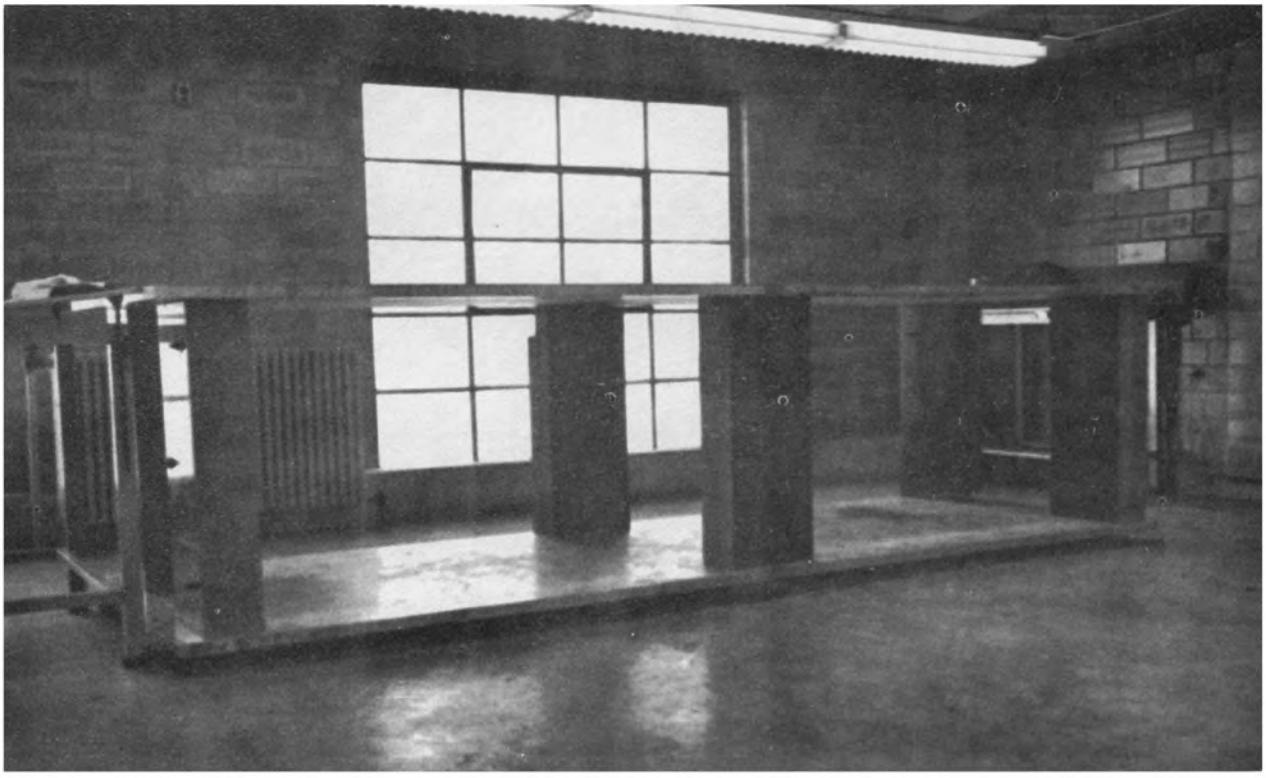

Fig. 2 The Table

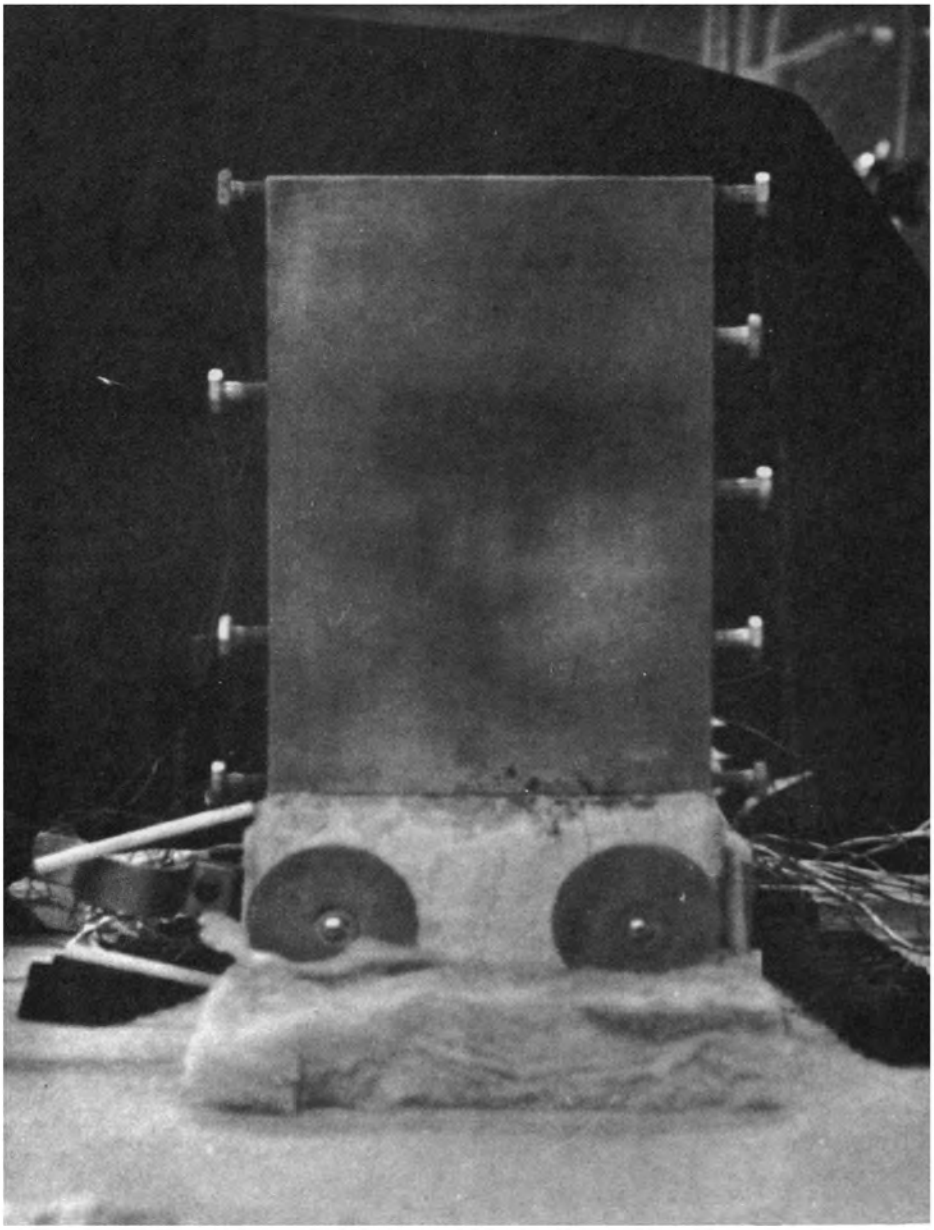

Fig. 3a. The Heated Plate

Fig. 3b. Thermocouple Jacket

brass. The lower two inches were machined down 1/16 inch on each surface. This was to allow for the installation of the heating element which consisted of 12 feet of nickel-chromium wire with a resistance of 5.6 ohms per linear foot, wrapped about the plate and sandwiched between two coats of plastic porcelain which electrically insulated the plate. The plate was then heated by passing various amounts of current through this wire.

The plate was equipped with nine thermocouples to measure the temperature along its length. One of the thermocouples was found to give faulty readings so no data was taken from it. Two sets of thermocouples were placed directly opposite one another to insure that the plate temperature was uniform across its width. This was necessary to insure that the problem was two dimensional. Had the temperature varied across the surface, the interference fringes would have represented the integral of that temperature distribution. The temperature was found to be uniform across the surface to within two degrees. This integration of temperature is not peculiar to this system. Nor is the stability requirement peculiar to this system,but rather, they are both characteristic of all interferometers.

The thermocouple jacket employed is pictured in Figure 3(b). It consists of a section of thin nickel tubing crimped at one end to prevent the thermocouple bead from sliding out. The other end is inserted in a drilled-out

machine screw and also crimped to prevent its sliding farther into the hole in the screw. This jacket can then be easily inserted and tightened until the thermocouple bead is pressed firmly against the bottom of the hole. This was found to be an effective, yet simple, way to insure accurate temperature measurement. The thermocouples were copper-constantan coated with teflon and the millivolts were measured by a Leeds and Northrup potentiometer with an ice bath reference junction.

The plate was bolted to an aluminum block as a means of securing it for photography. An attempt was made to insulate the block from the plate using a one inch thick fiberglass insulation, but as will be seen later, this attempt was not entirely successful. Other methods of suspending the plate were tried, but they all proved unsatisfactory. The primary characteristic which led to changing methods was the lack of stability. The object cannot move one-half of a wave length of the illuminating light or the fringes will be destroyed. Again, stability is of primary importance in holography.

3. The Optical Components

The optical components of the system are shown in their precise locations with respect to each other in Figure 4. The actual theory of operation will be described in detail in the next section. The optical components consist of a

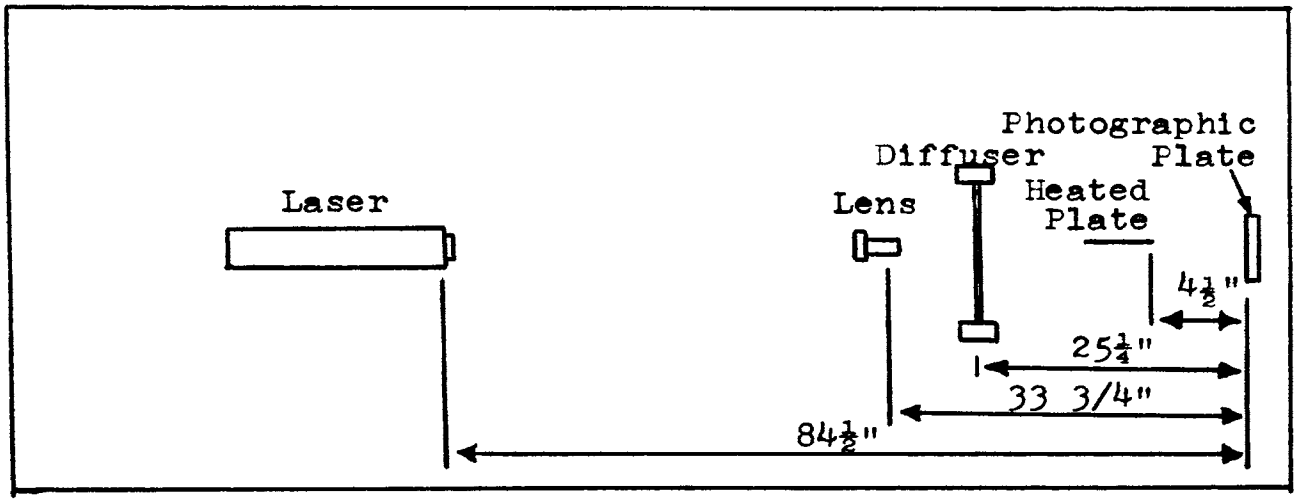

a) Top view

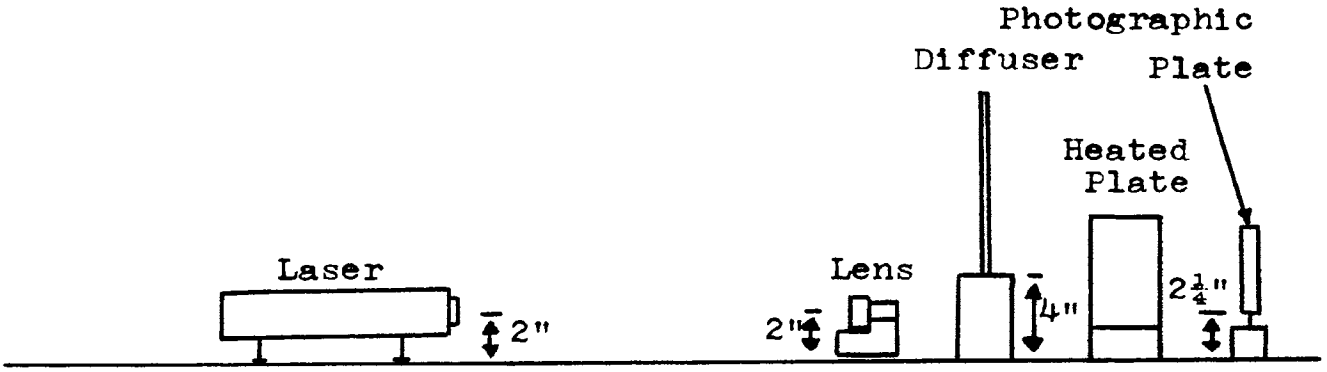

b) Side view

Fig. 4 Table Layout Sketch

Spectra-Physics model 124 helium-neon gas laser which has a wavelength of 6328 Angstroms, a 100 power microscope objective lens, a 20 inch by 10 inch piece of sand-blasted window glass, and a 5 inch by 4 inch photographic plate holder. A photograph of the table layout appears in Figure 5.

B. Experimental Procedure

A detailed explanation of holographic theory will not be included here. If the reader is unfamiliar with holography, it is recommended that he consult the literature[7,8], although this will not be necessary in order to understand the following discussion.

The holographic process consists of two steps: recording and reconstruction. In the recording process a double exposure hologram is made. First, an exposure of the unheated apparatus is taken. The sand-blasted window glass serves to diffusely illuminate the object and eliminate the one-to-one correspondence between the object and the hologram. This means that the entire object can be seen from any single location. Before this idea was introduced by Leith and Upatnieks[8], it was necessary to use special optical aids to view the entire object simultaneously. The illuminated window glass also provides a uniform background illumination for viewing the fringes. A portion of the beam passes under the diffuser striking the object or proceeding

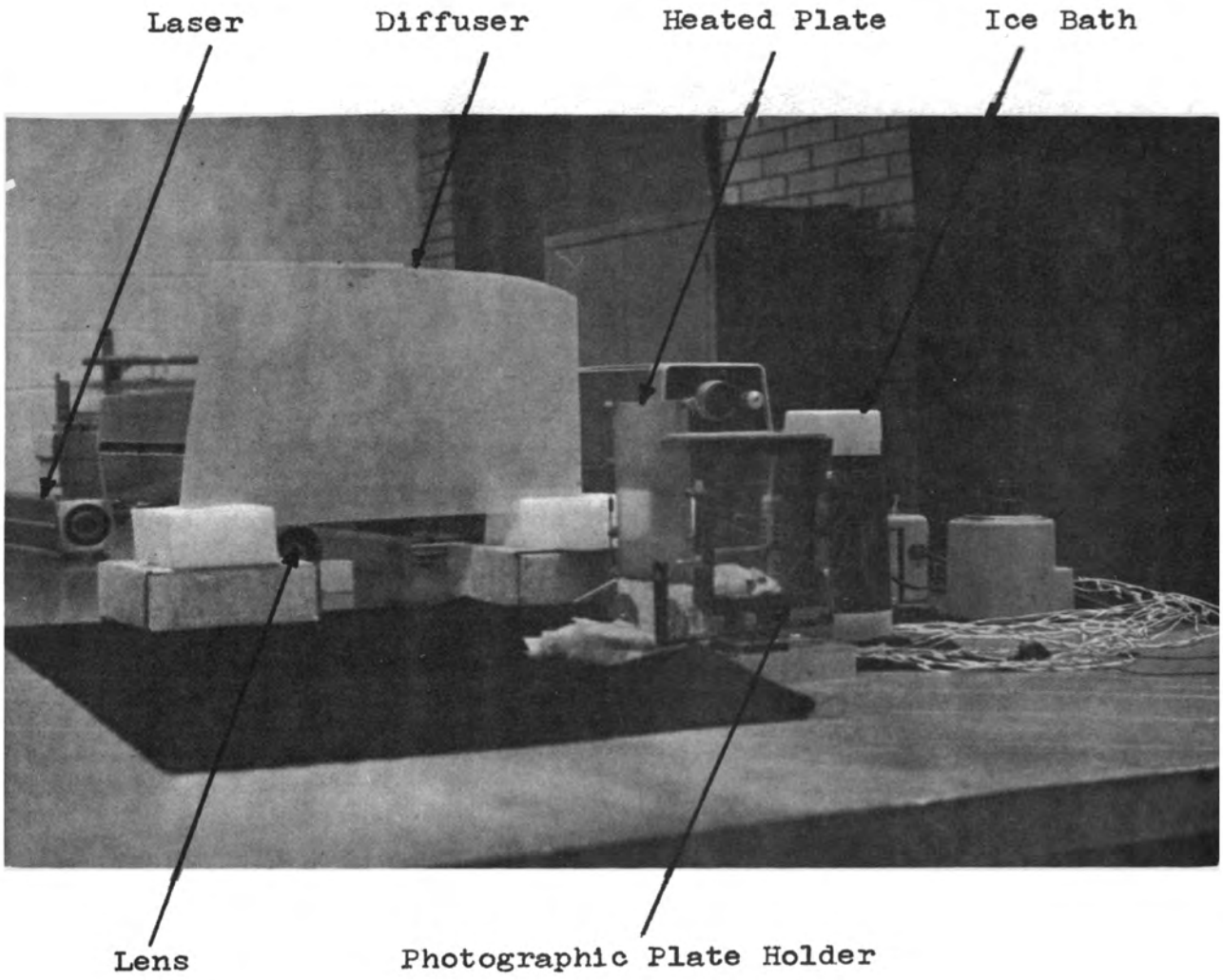

Fig. 5 Table Layout Photograph

directly to the photographic plate. This initial exposure serves as a reference exposure. The second exposure is made after the heated plate reaches thermal equilibrium. Since the heated plate has caused a density change in the air about the plate, the light beam is bent in the disturbed region, and the interference with the reference exposure causes the formation of the fringes.

The second step is the reconstruction. Once the hologram has been developed, it is replaced in its holder and illuminated by the reference beam. The object image will be three dimensional and appear to be in the same location as when the hologram was made. That is, unlike conventional photography, the image will not appear on the surface of the hologram but will be located in the original object position. The fringes will also appear in their 3-dimensional locations relative to the heated plate. The real image is vertically separated from the virtual image in this system and does not interfere with the viewing of the virtual image.

Agfa-Gevaert photographic plates were used to make the holograms with a 1 1/2 second exposure time (three seconds total). The photographs were taken with a Miranda Fv 35mm camera using ASA32 film, a time exposure of 2 1/2 minutes, and a telephoto lens. The ability to focus on the fringes was increased by the use of lens extensions. A larger spectra-Physics model 125 laser was used for reconstruction. This was not actually necessary to observe the information but was done in order to achieve better quality photographs.

These fringes were recorded using a comparatively inexpensive, low power laser and a 100 power microscope objective. There are no high quality optical components required, no precision alignment, and a dust free environment is by no means essential. Any dust particles or scratches on the lens are obliterated by the diffuser plate. The images of the dust particles and lens aberrations that are recorded by the photographic plate, are inconsequential since the information is not viewed on the plate surface, but behind it. Nor are optically perfect windows required on the test section, since the holographic interferometer senses only the transient event and will ignore the non-homogenities, which remain constant. If the optical properties of the windows vary in the temperature range under investigation, and this variation is known, the fringe information can be corrected to give the information desired.

The size of the laser needed depends on the application. This Spectra-Physics Model 124 laser was used with an exposure time of 1 1/2 seconds to record a "steady state" phenomena. A higher powered gas laser or a pulsed laser would be needed in order to achieve shorter exposure times and capture the more transient phenomena, such as transitional or turbulent flow.

IV. THEORETICAL MODEL

In order to compare the photographic results with an established theory, it was necessary to construct a theoretical model. Although the wall temperature distribution can be described by a quadratic equation, it was necessary to assume an alternate distribution, since the complexity of the solution made the use of the quadratic untractable.

Beginning with the integral form of the momentum and energy equations for laminar free convective flow*

$$\frac{d}{dx}\int_o^\delta u^2 dy = gB\int_o^\delta (T - T_\infty)dy - \nu\left(\frac{du}{dy}\right)\Big|_{y=0} \qquad (1)$$

$$\frac{d}{dx}\int_o^\delta u(T - T_\infty)dy = -\alpha\left(\frac{dT}{dy}\right)\Big|_{y=0} \qquad (2)$$

In using these equations, it has been assumed that the flow is laminar, two dimensional, with constant properties. It has also been assumed that the conduction term for the x-direction can be neglected. These assumptions are accurate for this analysis.

The boundary conditions governing these equations are

$$T = T_\infty,\ u = 0 \text{ at } x = 0$$

$$T = T_w(x),\ u = 0 \text{ at } y = 0$$

*A list of all symbols may be found at the beginning of the thesis.

$$T = T_\infty,\ u = 0 \text{ at } y = \delta \tag{3}$$

$$\frac{dT}{dy} = 0,\ \frac{du}{dy} = 0 \text{ at } y = \delta$$

If the boundary conditions on temperature are used to solve an assumed polynomial, it is found that the expression governing the temperature distribution is

$$T - T_\infty = (T_w(x) - T_\infty)(1 - \frac{Y}{\delta})^2 \equiv \theta_w(x)(1 - \frac{Y}{\delta})^2 \tag{4}$$

Likewise, if the boundary conditions on the velocity are used to solve a cubic polynomial, the velocity profile it is found to have the form

$$\frac{u}{w} = \frac{Y}{\delta}(1 - \frac{Y}{\delta})^2 \tag{5}$$

For this particular model, the temperature distribution is

$$\frac{\theta_w(x)}{\theta_{w_o}} = 1 \pm A(\frac{x}{L})^r \tag{6}$$

According to Sparrow[9], the value of A should be the maximum percent deviation from θ_{w_o}. However, since this is a forced fit curve, if this value of A is used the other points on the curve are not adequately described by this equation. Therefore, a least squares approach was used. If this is done, then two non-linear equations for A are obtained, expressed as constants raised to the r power.

These equations can be solved by trial and error or by computer. When a value for r produces the same value for A from each of the equations, then the least squares fit has been determined.

If the expressions for the velocity and temperature distribution are substituted into equations (1) and (2) and the integration is carried out, the following differential equations result

$$\frac{1}{105}\frac{d}{dx}(w^2\delta) = gB\theta_{w_o}\left[1 - A\left(\frac{x}{L}\right)^r\right]\frac{\delta}{3} - \frac{\nu w}{\delta} \qquad (7)$$

and

$$\frac{1}{30}\frac{d}{dx}\left\{w\delta\left[1-A\left(\frac{x}{L}\right)^r\right]\right\} = \frac{2\alpha}{\delta}\left[1 - A\left(\frac{x}{L}\right)^r\right] \qquad (8)$$

This result is very similar to the result that appears in reference (3) for the constant wall temperature case, with the exception that the temperature distribution may not be taken outside the derivative in equation (8) and canceled with the like expression on the other side.

If δ and w are represented by a power series in A, that is

$$\delta = \delta_o + \frac{A\delta_1}{1!} + \frac{A^2\delta_2}{2!} + \ldots \qquad (9)$$

and

$$w = w_o + \frac{Aw_1}{1!} + \frac{A^2w_2}{2!} + \ldots \qquad (10)$$

then these expressions can be substituted into equations (7) and (8). If each resulting equation for each power of A is equated to zero, then the coefficient of A must identically be equal to zero since A is not equal to zero for the non-uniform wall temperature case.

The equations for the A^o term are

$$\frac{1}{105}\frac{d}{dx}[w_o^2\delta_o] - 1/3gB\theta w_o\delta_o + \nu\frac{w_o}{\delta_o} = 0 \qquad (11)$$

$$\frac{1}{30}\frac{d}{dx}[w_o\delta_o] - \frac{2\alpha}{\delta_o} = 0 \qquad (12)$$

Now, assume that $\delta = Cx^m$, $\delta_o = C_o x^m$ (13)

$$w = Dx^n, \quad w_o = D_o x^n \qquad (14)$$

Once this form is used, constants C_o, D_o, m and n are determined by substituting equations (13) and (14) into equations (11) and (12). Since each term must have x to the same power, m and n are 1/4 and 1/2, respectively. C_o and D_o can now be found. The expressions for C_o and D_o are

$$C_o = 3.93(Pr)^{-1/2}\left(\frac{20}{21} + Pr\right)^{1/4}\left[\frac{gB\theta Bw_o}{\nu^2}\right]^{-1/4} \qquad (15)$$

$$D_o = 5.165\nu\left(\frac{20}{21} + Pr\right)^{-1/2}\left[\frac{gB\theta w_o}{\nu^2}\right]^{1/2} \qquad (16)$$

which are seen to be the solutions to the constant wall temperature problem. (It should be mentioned here that in

the numerical solution to these equations, a $\overline{T}$ is used which is equal to one half the sum of the average plate temperature and ambient temperature.)

If a similar procedure is followed for the A^1 equations (and here one must substitute his θ_w expression numerically) it is found that the resulting differential equations are

$$\frac{1}{105}\frac{d}{dx}\left[w_o^2\delta_1 + 2w_o w_1\delta_o\right]\delta_o + \frac{1}{3}gB\theta_{w_o}\delta_o\delta_1$$

$$-\nu\frac{w_o}{\delta_o}\delta_1 - \frac{2}{3}gB\theta_{w_o}\delta_o\delta_1 \mp \frac{1}{3}gB\theta_{w_o}\left(\frac{x}{\overline{L}}\right)^r\delta_o^2 \qquad (17)$$

$$+\nu w_1 = 0$$

and

$$\frac{1}{30}\frac{d}{dx}\left[w_o\delta_1 + \delta_o w_1 \pm w_o\delta_o\left(\frac{x}{\overline{L}}\right)^r\right]\delta_o + \frac{2\alpha}{\delta_o}\delta_1$$

$$\mp 2\alpha\left(\frac{x}{\overline{L}}\right)^r = 0 \qquad (18)$$

So,

$$p = r + \frac{1}{4} \quad \text{and} \quad s = r + \frac{1}{2}$$

where p and s are defined by

$$\delta_1 = C_1 x^p$$
$$w_1 = D_1 x^s \qquad (19)$$

Solving equation (18) for D_1 in terms of C_1, and then substituting in equation (17) and solving for C_1, produces an equation of the form

$$C_1 = \frac{(\frac{1}{L})^r [\pm \frac{1}{3}gB\theta_{w_o} C_o^2 + \frac{120\alpha}{105} (\frac{1+P}{\frac{1}{2}+P}) D_o \pm \frac{2(1+P)}{105} C_o^2 D_o^2 \mp \frac{60\alpha\nu}{(P+\frac{1}{2}) C_o^2} + \nu D_o]}{-\frac{1}{C_o} [1/3gB\theta_{w_o} C_o^2 + \frac{120}{105}(\frac{1+P}{\frac{1}{2}+P}) D_o + (\frac{1+P}{105}) C_o^2 D_o^2 + \frac{60\alpha\nu}{(P+\frac{1}{2}) C_o^2} + 2\nu D_o]} \quad (20)$$

The lower set of signs are used if there is a negative sign in the $\theta_w(x)$ expression, whereas the upper set of signs are used if a positive sign appears in the expression.

This equation appears highly untractable at first glance. However, when numerical values were substituted into this expression, it was found that the second and fourth terms are generally four orders of magnitude larger than the other terms and these other terms may then be neglected. For the choice of the lower set of signs (a decaying thermal distribution), the two terms in brackets reduce to a value of one, and C_1 can be expressed simply as

$$C_1 = - (\frac{1}{L})^r C_o \quad (21)$$

This expression can then be used to solve for D_1. This is not done here since the primary interest is in the thermal boundary layer. This value for δ

$$\delta = \delta_o + A\delta_1 = C_o x^m - A(\frac{1}{L})^r C_o x^p \qquad (22)$$

represents the first approximation for this variable wall distribution. For better approximations more A equations must be solved for the C's and D's and the exponents on x. This first correction term represents less than a twenty-five percent correction factor, so the next higher order term will probably adjust the boundary layer thickness by only five percent. According to Sparrow, the next correction will be an additive term and adjust the value for δ back towards the value for the isothermal wall.

It must be noted here that this analysis does not agree with the one presented by Sparrow[9]. In defense of these results, it must also be noted that Sparrow's results also are in contradiction with the isothermal wall results, while these findings are in complete agreement with that solution. Sparrow's results suggest that the isothermal wall boundary layer thickness should be proportional to $x^{1/5}$ and the velocity boundary layer proportional to $x^{3/5}$. It is out of the realm of possibility for this author to find himself in direct contradiction of Sparrow, so it will be assumed that his erroneous exponents are misprints.

The integral method for the isothermal case agrees with the exact solution to the differential equations[10] to within 6.5%. This suggests that this method, as applied

to the non-isothermal wall case, should have an accuracy within 10%, which is indeed acceptable.

V. RESULTS AND DISCUSSION

The data has been formally presented in Table I. The millivolt reading, along with the corresponding temperature, is listed for each thermocouple for each of the four holograms. The "x value" row is the distance in inches between thermocouple number one and that particular thermocouple. The "exp. θ_w/θ_{w_o}" is the temperature distribution of the plate as it was measured, while the "theory value" is the value given by the equation listed directly above each block. These are the equations used in the construction of the theoretical model. It is worthwhile to point out that the maximum deviation between the theory and the experiment is less than four percent.

Figures 6 through 9 are the photographs of the boundary layers for the four holograms. Several interesting traits may be noted. First, the left hand boundary layer is thicker than the right and contains one or two additional fringes. Second, the right hand boundary layer has irregular disturbances occuring in the free stream area, while the left hand boundary layer seems to sweep horizontally out into the free stream.

To understand these peculiarities it is necessary to refer to Figure (3a). In the lower portion of the plate on the heating element section, it will be noted that two large

TABLE I. DATA

Thermocouple	1	2	3	4	5	6	7	9
x value (in)	0	.0313	1.44	1.44	2.91	3.81	4.375	5.75
Plate No. 1 Amb. 72F $\theta_w = 420\,[1 - .247(\frac{x}{L})^{.59}]$								
M.V. reading	12.34	12.105	11	10.98	10.14	9.686	9.546	9.401
Temperature F	492.7	484.9	449	448.9	420.6	405.4	400.7	395.8
Exp. θ_w/θ_{wo}	1	.983	.898	.898	.829	.794	.783	.770
Theory value	1	.987	.891	.891	.835	.806	.790	.753
Plate No. 2 Amb. 71F $\theta_w = 338\,[1 - .237(\frac{x}{L})^{.58}]$								
M.V. reading	9.814	9.712	8.808	8.776	8.18	7.81	7.734	7.601
Temperature F	409.7	406.3	375.7	374.6	354.1	341.2	338.5	333.9
Exp. θ_w/θ_{wo}	1	.991	.901	.901	.838	.799	.791	.778
Theory value	1	.988	.894	.894	.839	.813	.797	.763
Plate No. 3 Amb. 70F $\theta_w = 223\,[1-.2268(\frac{x}{L})^{.56}]$								
M.V. reading	6.43	6.343	5.845	5.846	5.478	5.296	5.227	5.162
Temperature F	292.6	289	270.9	270.9	257.3	250.6	248	245.6
Exp. θ_w/θ_{wo}	1	.982	.901	.901	.840	.810	.798	.787
Theory value	1	.989	.896	.896	.845	.820	.805	.773
Plate No. 4 Amb. 72F $\theta_w = 128\,[1-.2237(\frac{x}{L})^{.55}]$								
M.V. reading	3.964	3.91	3.674	3.659	3.418	3.365	3.328	3.28
Temperature F	199.9	197.8	188.5	188.5	187.9	176.3	174.8	172.9
Exp. θ_w/θ_{wo}	1	.983	.906	.906	.831	.815	.803	.788
Theory value	1	.987	.896	.896	.846	.822	.807	.776

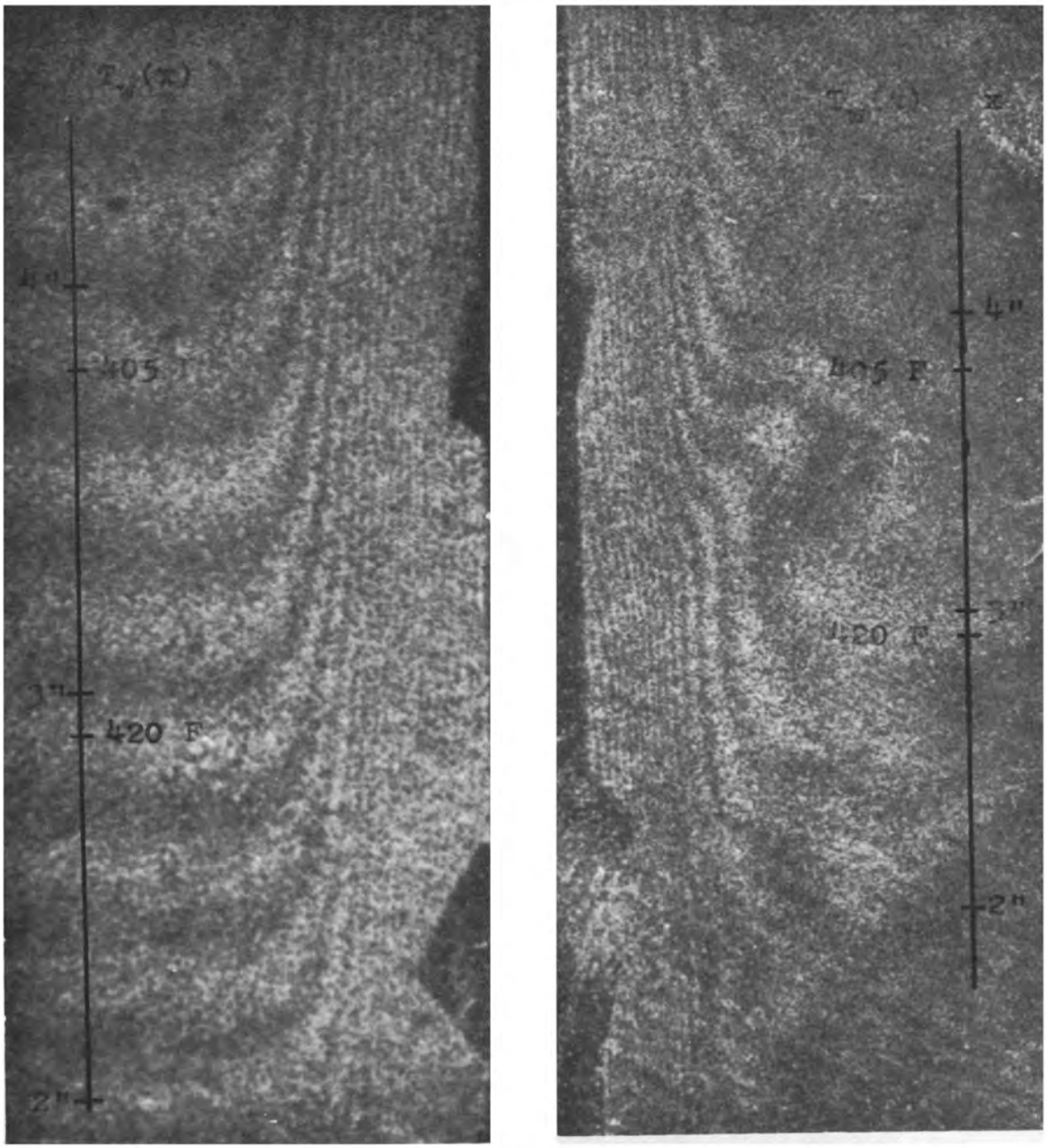

a) Left side

b) Right side

Fig. 6 Boundary Layer for Plate 1

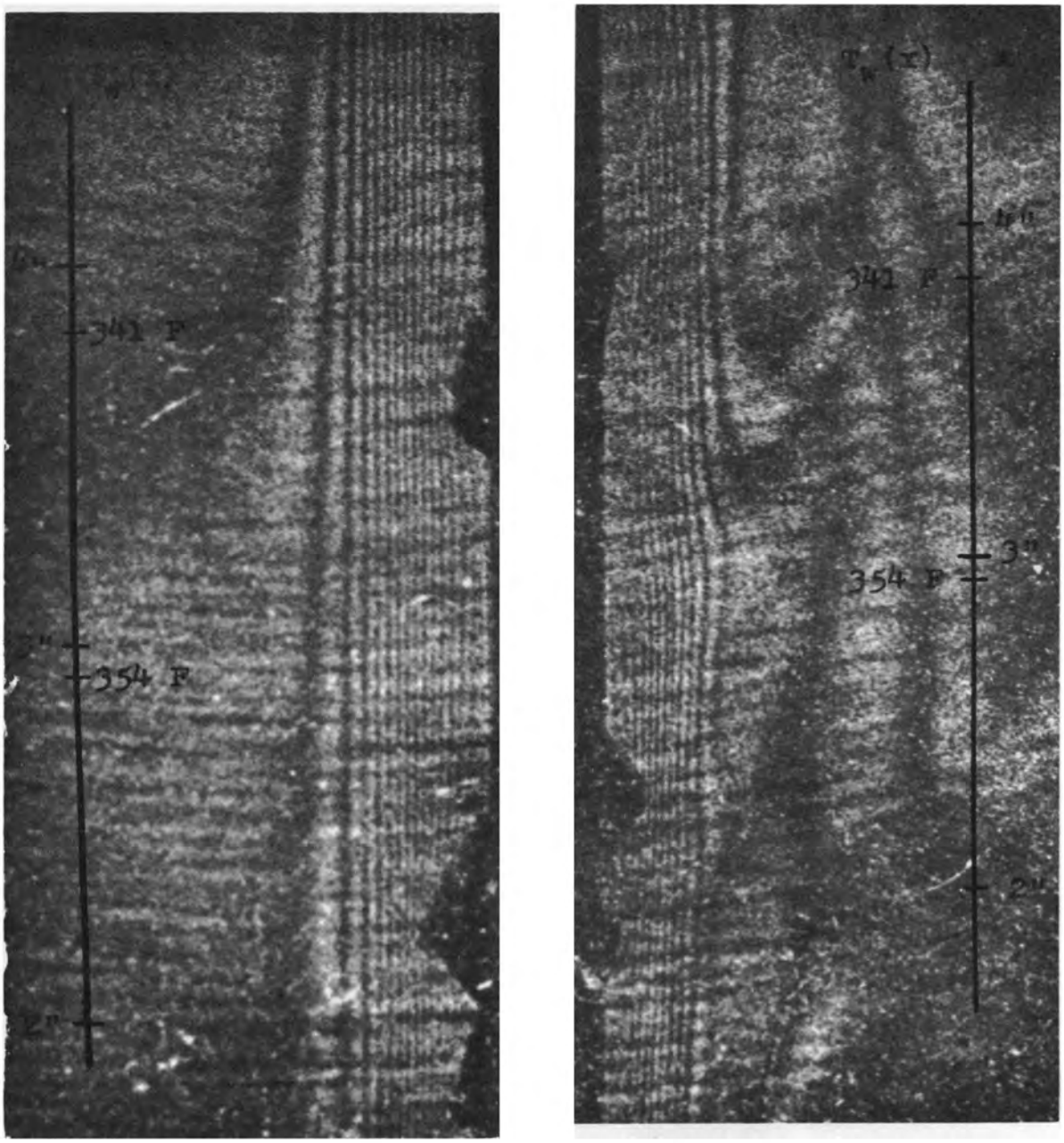

a) Left side

b) Right side

Fig. 7 Boundary Layer for Plate 2

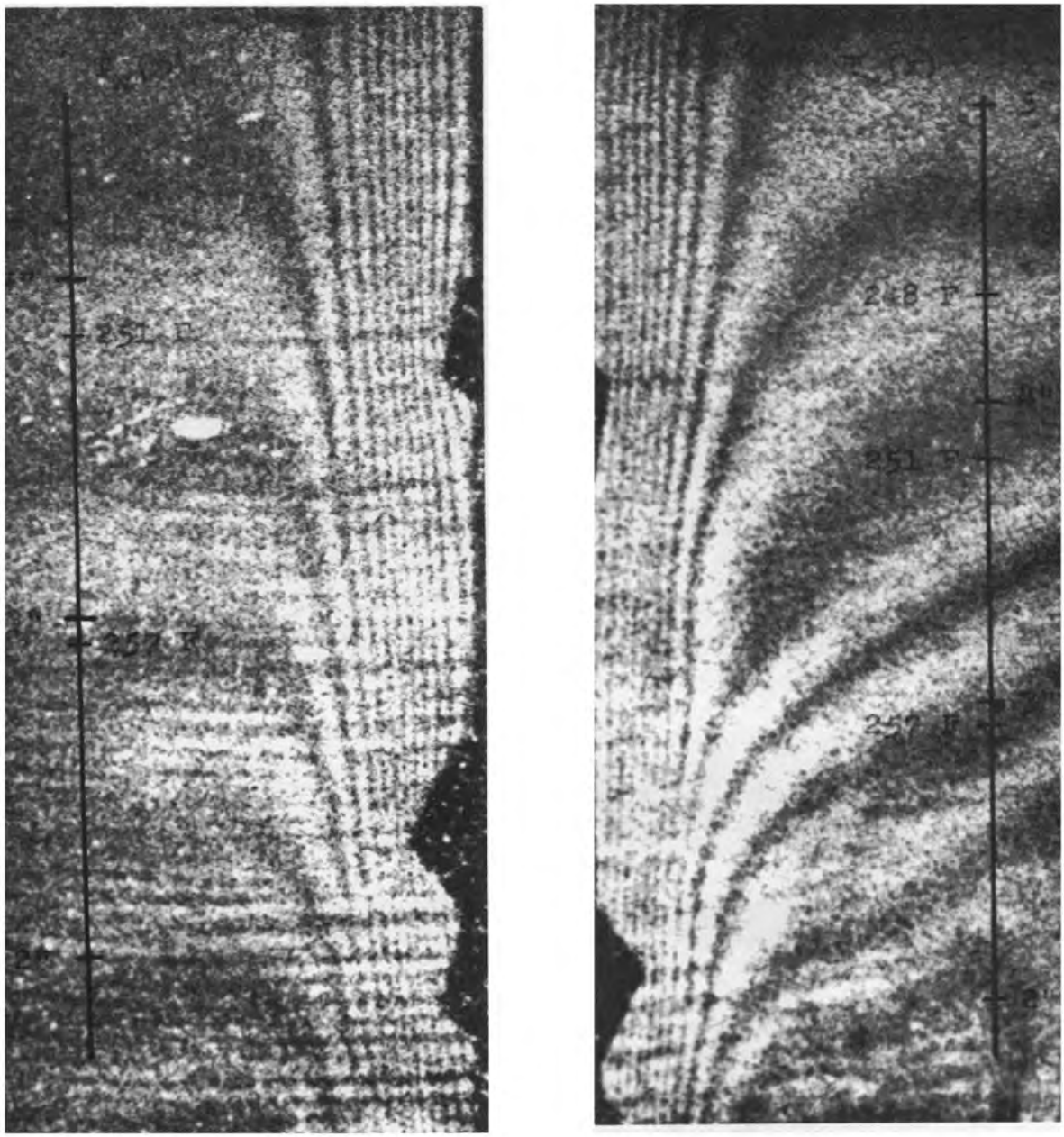

a) Left side

b) Right side

Fig. 8 Boundary Layer for Plate 3

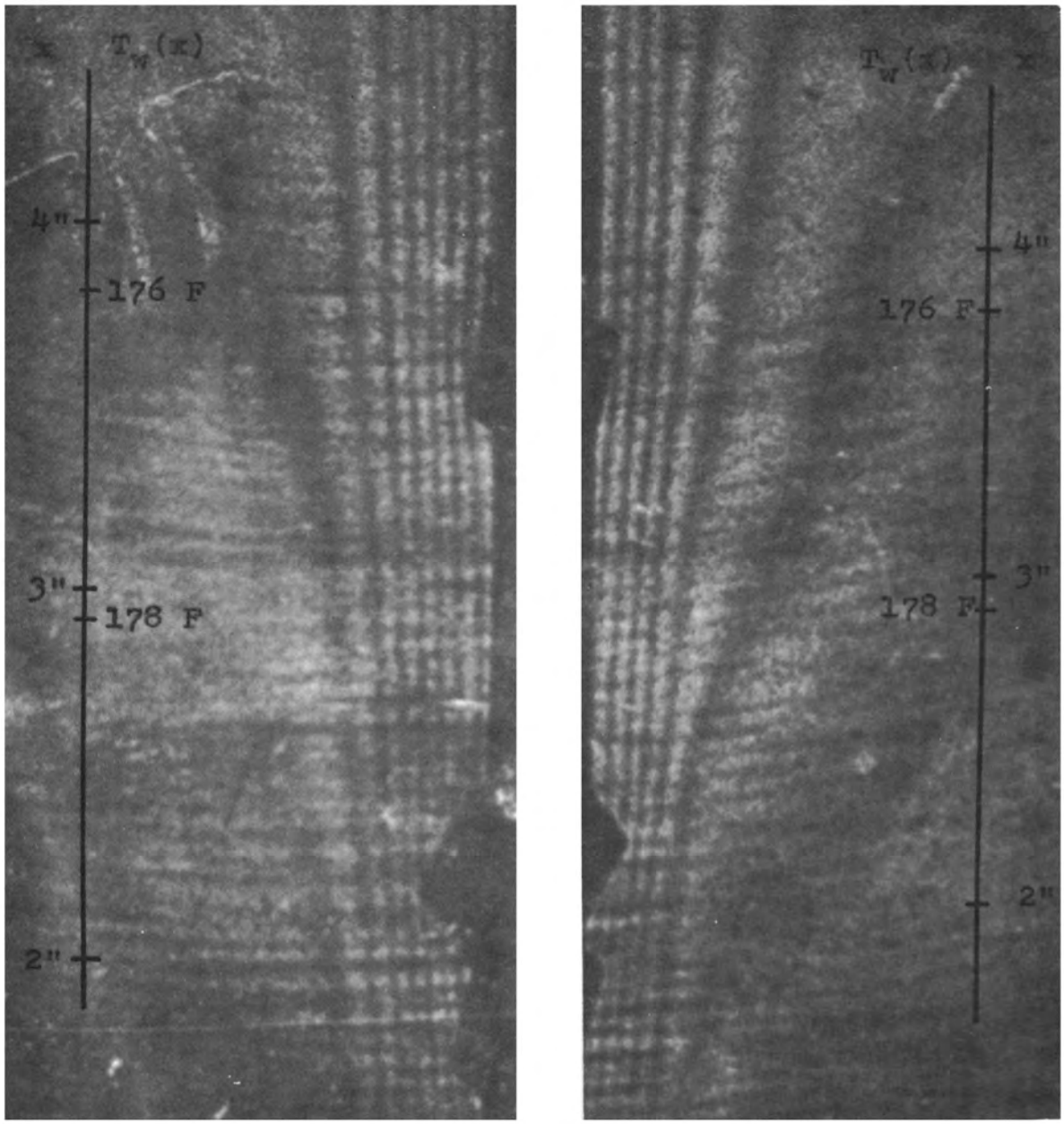

a) Left side

b) Right side

Fig. 9 Boundary Layer for Plate 4

washers have been used in the mounting of the plate. These two washers, along with the plastic porcelain, act as radiators of heat. Since the heating element must be considerably hotter than the highest temperature measured by the thermocouples, the element heats air several inches out from its surface. This has the consequence of thickening the boundary layer, and the air beyond the plate boundary layer merely cools as it rises. The fact that the constant temperature lines are thicker in this region indicates that the temperature is changing less rapidly, as would be expected. This effect is only observed on the left hand side of the plate.

The right hand side of the plate has a different set of characteristics since a different set of events is occurring there. The right hand side of the heating element is fastened through one inch of insulation to an aluminum block. The upper surface of the block also has a section of insulation covering it. However, in spite of these precautions, the block did become heated and the heat rising off the block caused a skewing of the boundary layer.

Figure (10 through 13) are sketches of the actual and theoretical boundary layers for each plate. These sketches are actual size. The expressions for δ used in making the sketches, and which were derived from the theoretical model, are indicated on each drawing. The tick marks indicate the locations of the thermocouples.

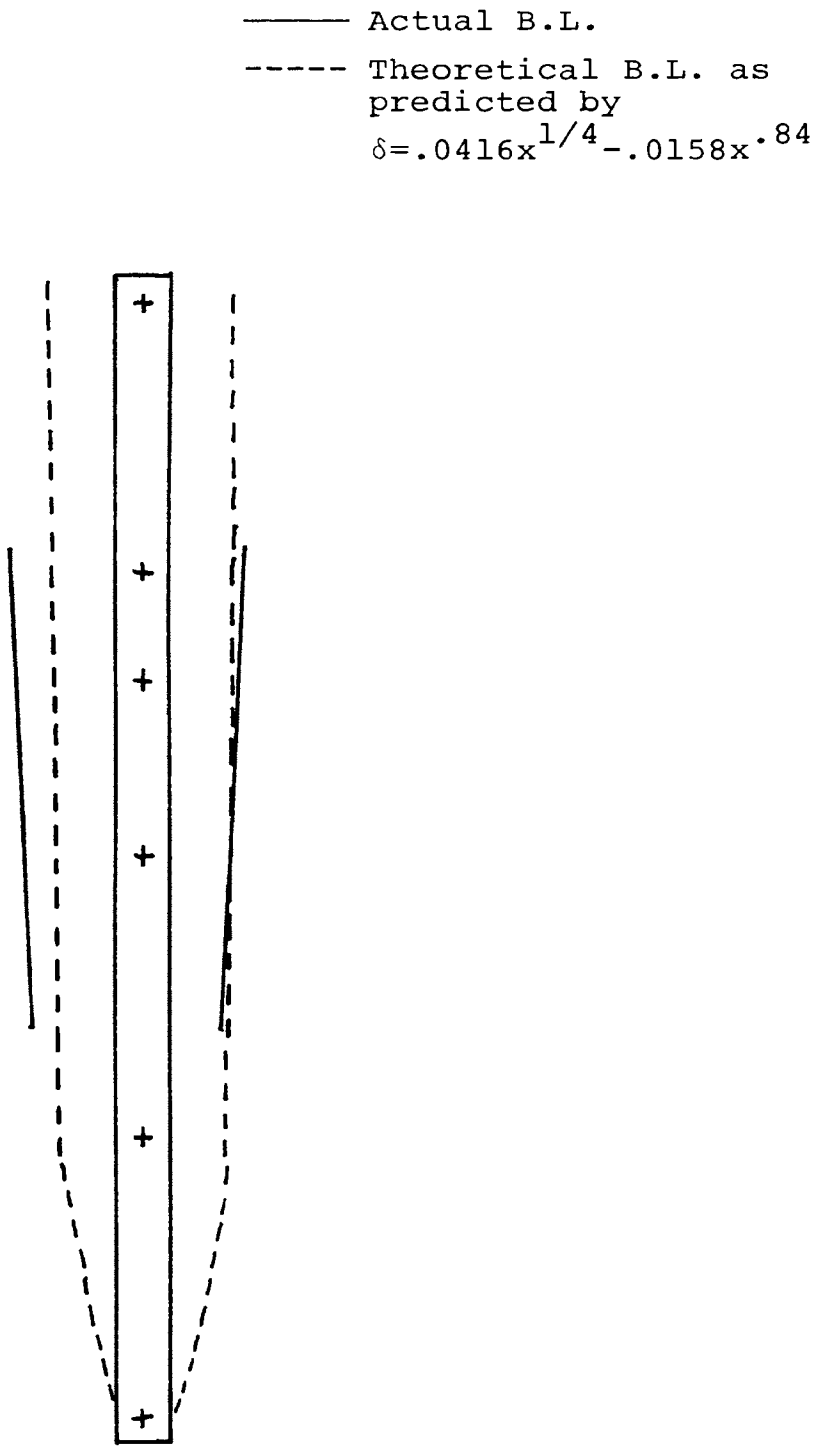

Fig. 10 Comparison Sketches for Plate 1

——— Actual B.L.

----- Theoretical B.L. as predicted by $\delta = .0415x^{1/4} - .01508x^{.83}$

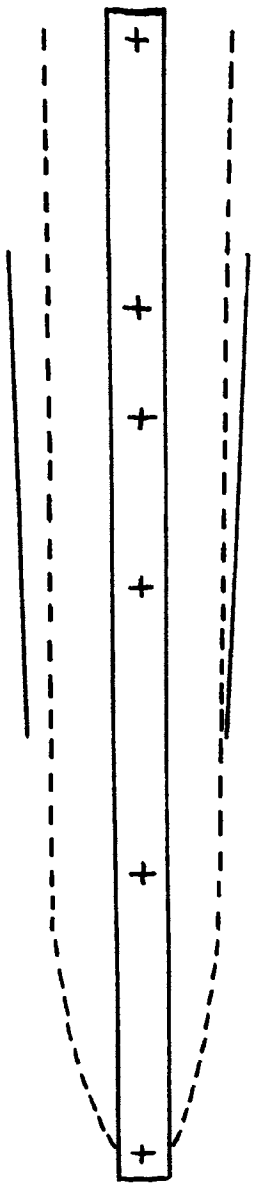

Fig. 11 Comparison Sketches for Plate 2

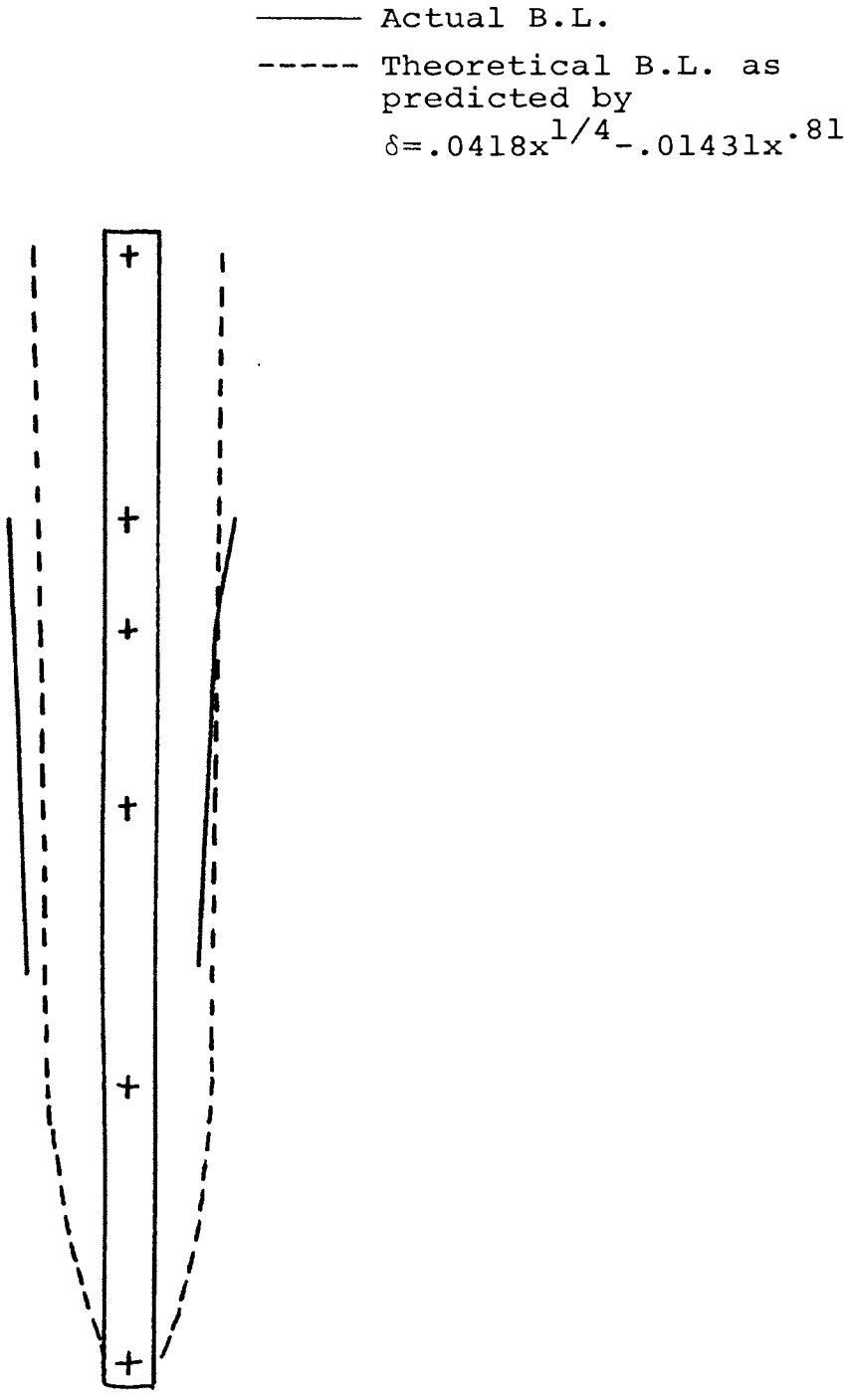

Fig. 12 Comparison Sketches for Plate 3

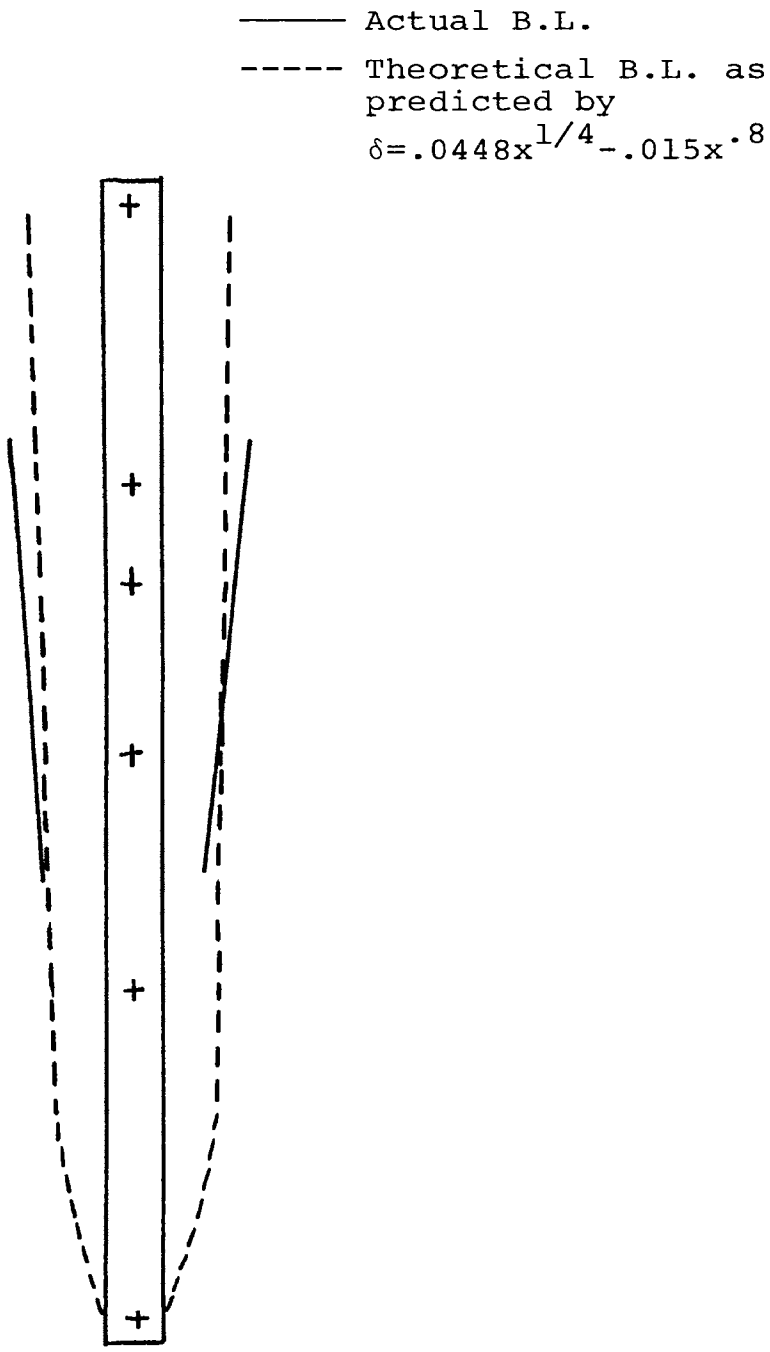

Fig. 13 Comparison Sketches for Plate 4

The reader is reminded that the theoretical solution for δ is found using an approximate method and that the expressions used here are the first order approximations to that solution. The second order approximation, although varying only slightly from this solution, would be wider at the top since the correction terms are most influential for large x values. It is a consequence of this theory that the boundary layer goes to zero at $x = 0$ regardless of what conditions actually exist there.

The results are seen to agree quite well with the theoretical boundary layer on the right hand side. The left hand boundary layer is understandably thicker than the theoretical value, since additional heating is present that was not accounted for in the theoretical derivation. The amount of deviation from the thoery decreases in this region, as the plate temperature decreases because the percentage of overheating done by the heating element also decreases. On the other hand, the amount of deviation from theory increases with decreasing temperature on the right hand side. This is caused by the fact that as the convective boundary layer weakens, the heat rising from the aluminum block becomes more influential. When the boundary layer is thus disturbed, it is difficult to ascertain where the measurements should be made.

Once the measurements of δ have been made, a least squares approach may be followed in order to obtain an

expression for the variation of δ with x. For this analysis, it will be assumed that the theoretical model adequately describes the actual boundary layer thickness. Since

$$q_w(x) = - kA \left.\frac{dT}{dy}\right|_w = hA(T_w(x) - T_\infty) \frac{Btu}{hr} \qquad (23)$$

and the temperature distribution has the form

$$\frac{T-T_\infty}{T_w(x)-T_\infty} = (1 - \frac{y}{\delta})^2 \qquad (24)$$

then

$$\left.\frac{dT}{dy}\right|_w = - \frac{2}{\delta} (T_w(x) - T_\infty) \qquad (25)$$

Substituting this relation into (23)

$$-kA(- \frac{2}{\delta}) (T_w(x) - T_\infty) = hA(T_w(x) - T_\infty) \qquad (26)$$

so

$$h = \frac{2k}{\delta} \qquad (27)$$

Using the expression for δ for plate #1

$$h = \frac{2k}{.0416x^{1/4} - .0158x^{.84}} \qquad (28)$$

Evaluating k at $\bar{T} = \frac{T_{wa} + T}{2} = 258^{o}F$,

$$h = \frac{2(.0185)}{.0416x^{1/4} - .0158x^{.84}} = \frac{1}{1.125x^{1/4} - .427x^{.84}} \frac{BTU}{hr\text{-}ft^{2}\text{-}F} \tag{29}$$

The expression for the overall heat transfer rate becomes

$$Q = b\int_{o}^{x} q_{w}(x)\lambda x = -kb \int_{o}^{x} \frac{dT}{dy}\Big|_{w} dx \tag{30}$$

Substituting the expression for the temperature distribution

$$Q = b\int_{o}^{x} \frac{\theta}{\delta}\, dx = 2kb\int_{o}^{x} \frac{1-A(\frac{x}{L})^{r}}{.0416x^{1/4} - .0158x^{.84}}\, dx \quad \frac{BTU}{hr} \tag{31}$$

It is seen that once δ is known, the other parameters may be calculated.

Figure 14 through 17 are the plots of the temperature distribution in the boundary layer in dimensionless form, as given by the photographs versus the theoretical distribution as expressed by equation 24. The theory understandably varies from the results since it is calculated using an approximate solution for δ and does not take into consideration the additional heating which is occurring. It will be noted, however, that the general shapes of the curves do correspond quite well. Both the theory and the measurements are calculated for x=3 inches.

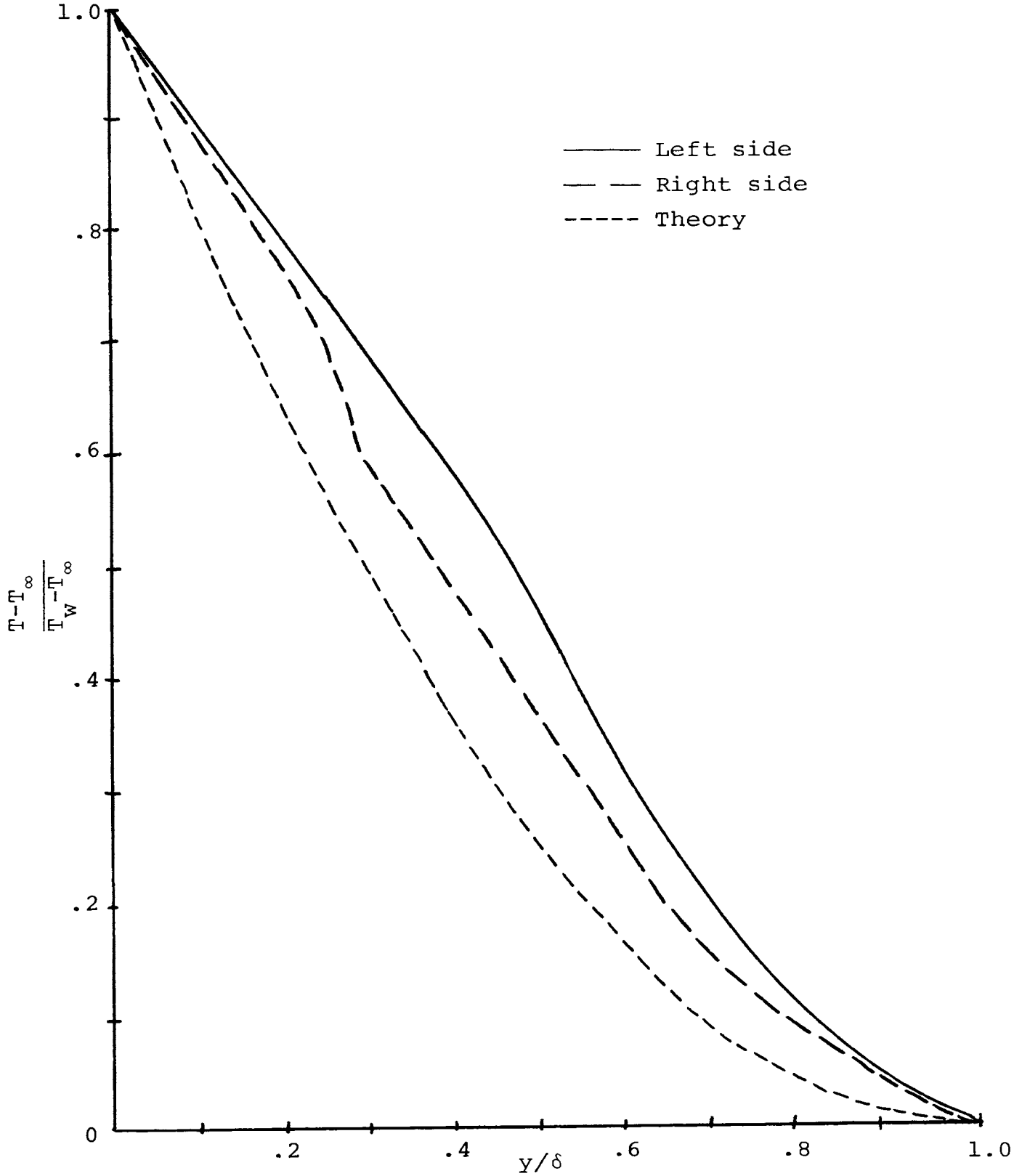

Fig. 14 Temperature Distribution in the Boundary Layer for Plate 1

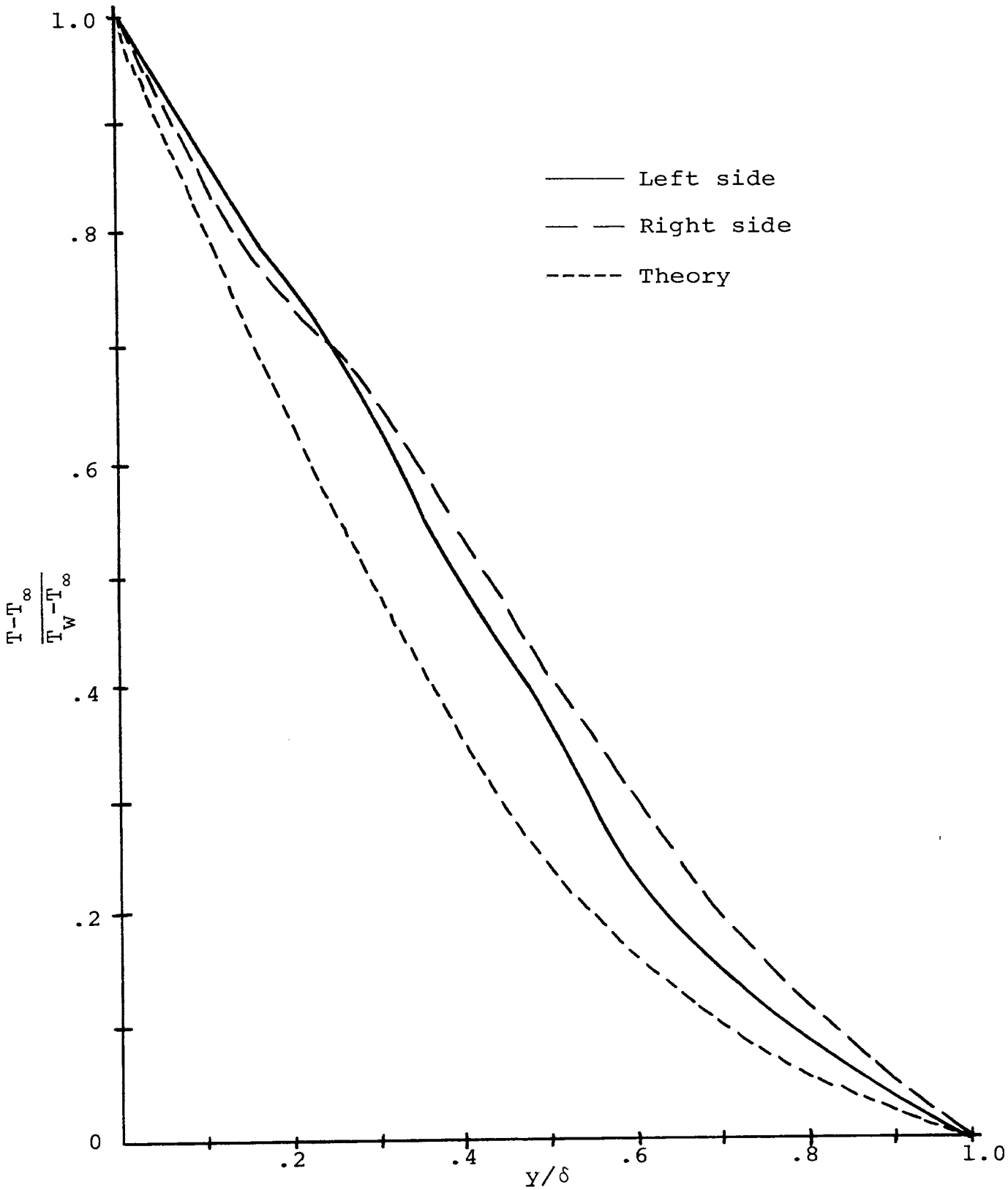

Fig. 15 Temperature Distribution in the Boundary Layer for Plate 2

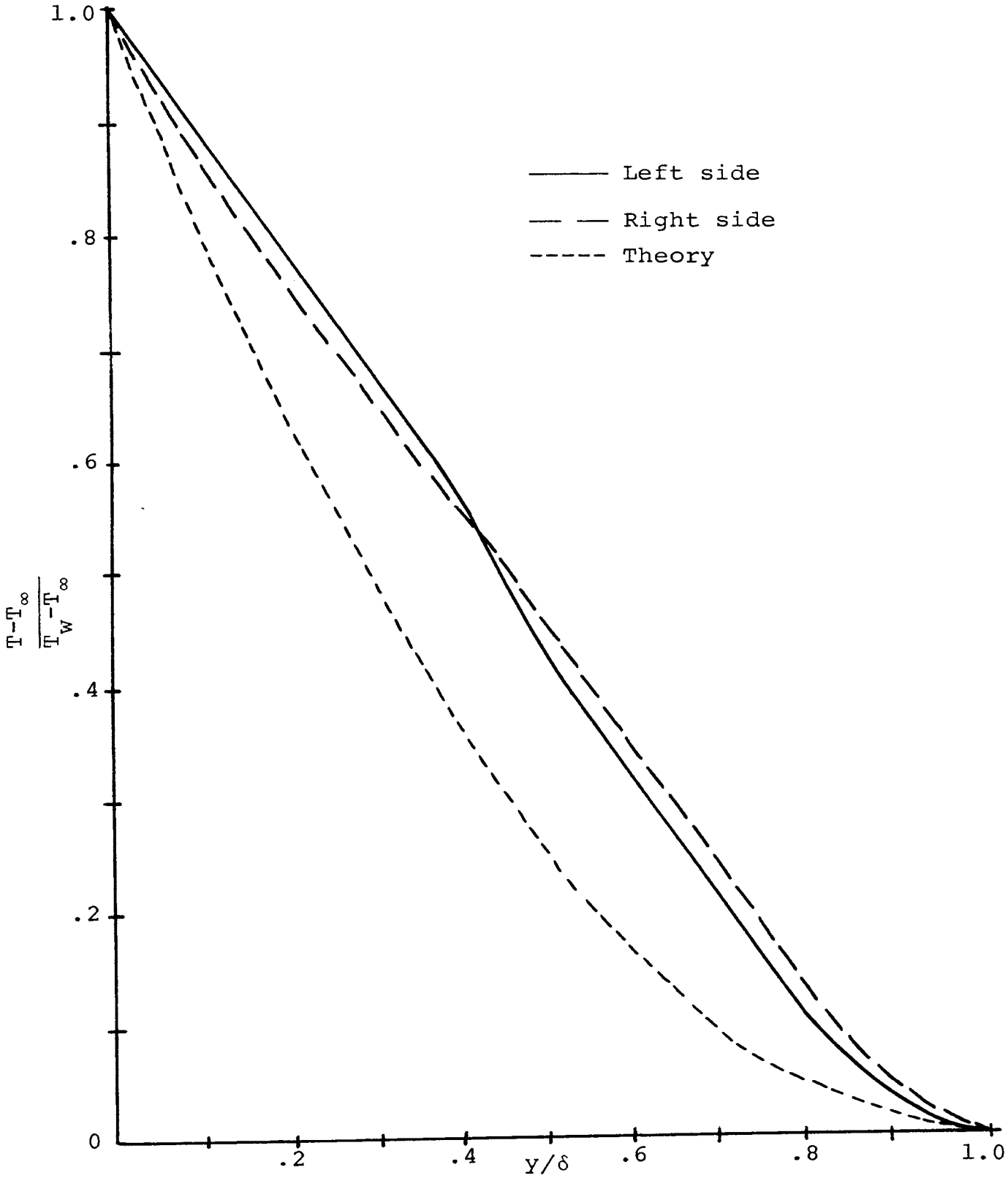

Fig. 16 Temperature Distribution in the Boundary Layer for Plate 3

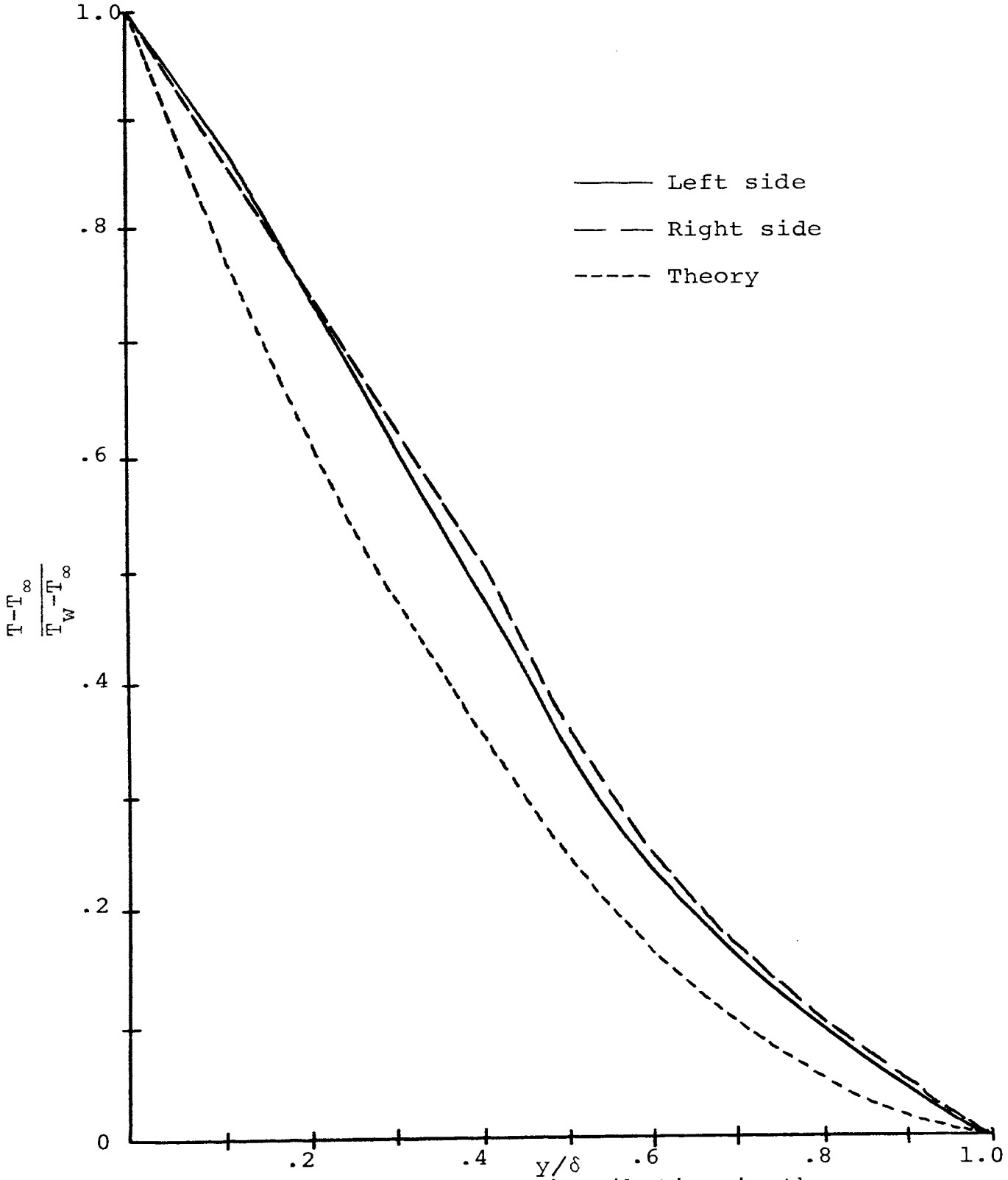

Fig. 17 Temperature Distribution in the Boundary Layer for Plate 4

A number of other interesting things may be observed from the photographs of the boundary layer. Since the plate temperature varies along its length, the constant temperature lines touch the plates. Therefore, the temperature which corresponds to each fringe may be found. These temperatures can be compared to those given by the Dale-Gladstone law and the equation of state for a perfect gas. Since the fringe thickness can be correlated to a temperature change, the heat transfer rate through the boundary layer is also known.

The Dale-Gladstone law also predicts the number of fringes for a given temperature drop $(T_w(x) - T_\infty)$. This means that if only the wave length of the laser and the depth of field are known, the plate temperature may be calculated by counting the number of fringes.

It was stated earlier that the holographic interferometer had the unique characteristic of being able to record everything that was occurring with a single exposure. Figure 18 is a photograph of a boundary layer which is actually in front of the heated plate. In Figure 3a, it can be seen that the wires emerging from the heating element are insulated by ceramic tubes. These ceramic tubes were heated to sufficiently high temperatures to cause the formation of the boundary layer pictured in Figure 18. It was recorded on the holographic plate simultaneously with the other boundary layers and appears in each of the holograms.

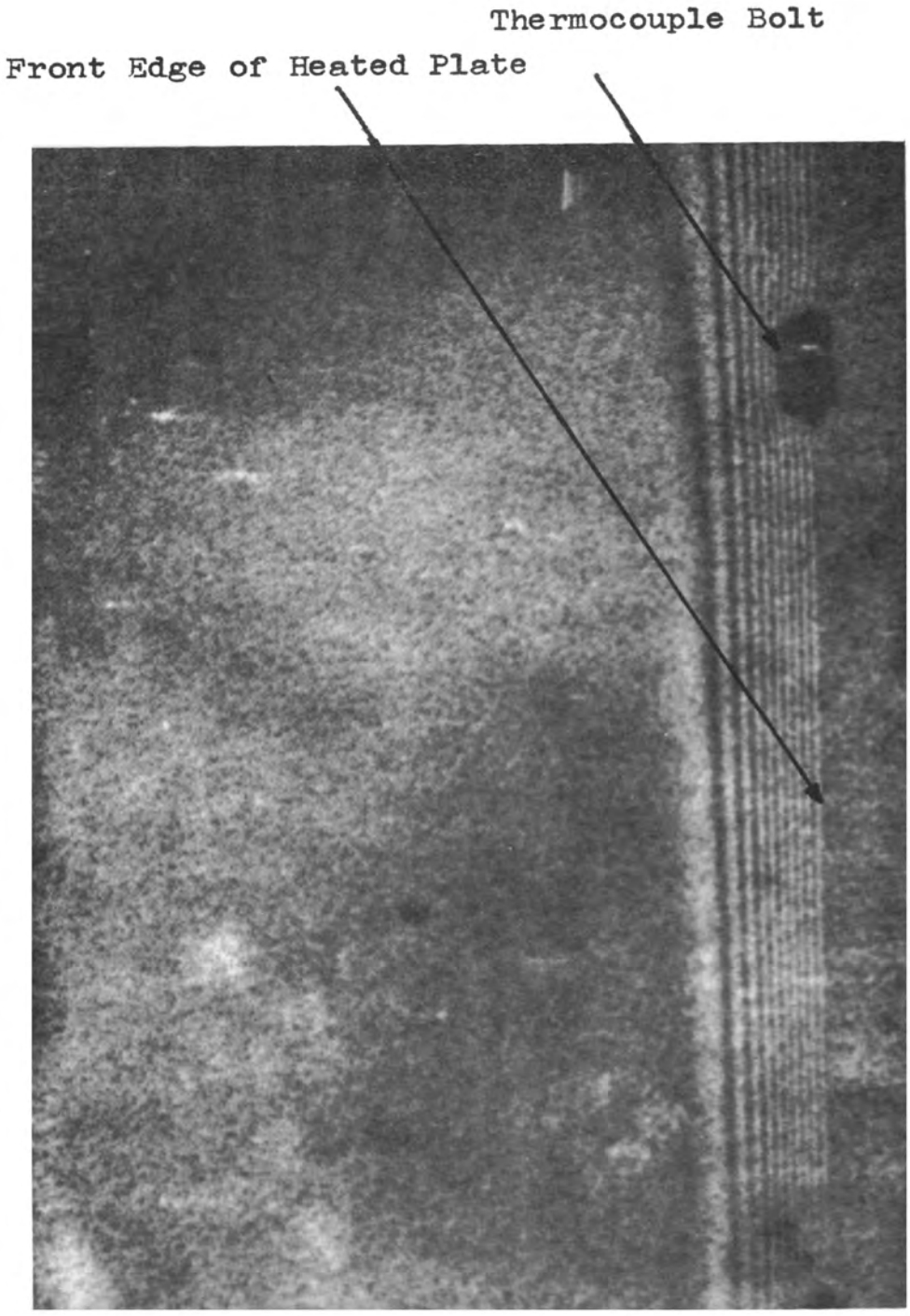

Fig. 18 Front Edge Boundary Layer

A number of the photographs indicate that fringes on the heated plate have been recorded. Figure 19 is one such photograph. These fringes are caused by the fact that there is a variation in temperature along the plate and the coefficient of thermal expansion causes a variation in optical path length. This phenomenon allows another unique characteristic of the holographic interferometer to be presented. With the proper optical design a combined convection-conduction problem could be studied: a capability of no other interferometer.

A final capability of the system has yet to be discussed. Thus far, only the double exposure holographic technique has been reported. The holographic interferometer has the ability to perform as a live fringe camera. In this technique, a single exposure of the unheated plate is made. After development, the hologram is reinserted in the holder in identically the same location. This alignment procedure does require more sophisticated equipment since the plate must be replaced in its exact location to within one-fourth of a wavelength in each of the three dimensions. Once this alignment has been achieved, however, the holographic interferometer may be used to watch the "live" development of the boundary layer. Since the eye is sometimes unable to detect rapidly changing phenomena, a motion picture camera should be used. In this way, the holographic interferometer could be used to

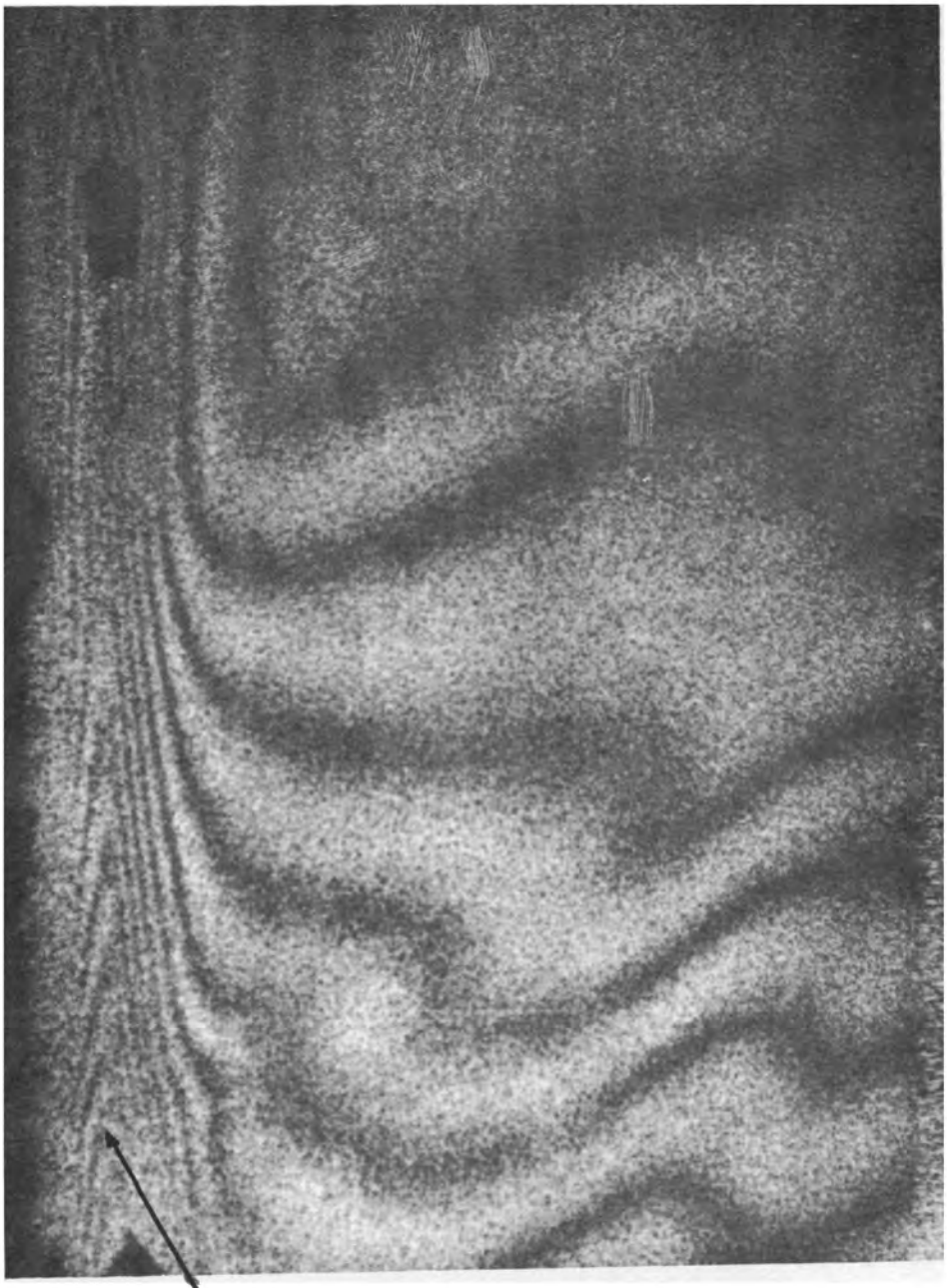

Fig. 19 Surfaces Fringes

detect such phenomena as transitional and turbulent flow which might otherwise require a pulse laser. The pulse laser would be capable of recording only a single event, whereas, the live fringe hologram could detect the entire sequence of events in a transient phenomenon.

VI. CONCLUSIONS

The results of this experiment indicate that the holographic interferometer has great utility as a temperature detecting device. Some of its major advantages are:

1) the capability of remote sensing, which is the ability to measure temperature without disturbing the boundary layer (this is a characteristic of all interferometers);

2) the inexpensiveness of this system compared to most other interferometers;

3) the ability to record three dimensionally everything that is occurring around the plate;

4) the fact that optically perfect and precision components are not needed;

5) the ability to use this instrument in spite of optical imperfections in the test section windows;

6) the fact that a dust-free environment is not needed;

7) the capability of simultaneously studying the combined conduction-convection problem;

8) the fact that precision alignment is not essential;

9) the high quality of the fringes obtained;

10) the ability to detect live fringes.

These are some of the characteristics that make this system potentially the most widely used interferometer available today.

VII. BIBLIOGRAPHY

1. Chen, P.L. Temperature Distribution in Thermal Boundary Layers (In Free Convection) Using a Modified Schlieren Method. UMR Thesis, 1965.

2. Hauf, W. and U. Grigull. "Optical Methods in Heat Transfer," Advances in Heat Transfer, Vol. 6, New York: Academic Press, 1970, 133-366.

3. Holman, J.P. Heat Transfer. New York: McGraw-Hill, 1968, 190-95.

4. Heflinger, L.O., and others. "Holographic Interferometry," Journal of Applied Physics, Vol. 37, No. 2, 642-49, Feb. 1966.

5. Powell, R.L. "Hologram Interferometry," Industrial Research, July, 1969.

6. Cutrona, L.J., and others. "Concepts and Uses of Pulsed Holography," Laser Focus, December, 1967.

7. Robertson, E.R., and J.M. Harvey (eds.). The Engineering Uses of Holography. Cambridge University Press, 1970

8. Smith, J.M. Principles of Holography. New York: John Wiley and Sons, 1969.

9. Sparrow, E.M. NACA TN 3508, (1955).

10. Ede, A.J. "Advances in Free Convection," Advances in Heat Transfer, Vol. 4, New York: Academic Press, 1967, 1-64.

VITA

Richard Kenneth Thomson was born on May 11, 1948 in Galveston, Texas. He received his elementary education in Whittier, California, and Darien, Connecticut, and his secondary education in Kirkwood, Missouri. He received his college education at the University of Missouri-Rolla in Rolla,Missouri where he received a Bachelor of Science Degree in Mechanical Engineering in May 1970.

He has been enrolled in the Graduate School at the University of Missouri-Rolla since June 1970 and has been supported by a Themis research grant under the direction of Dr. J. Kassner for the period June 1970 to July 15, 1971.